AGU PUBLICATIONS

JGR

Journal of Geophysical Research: Earth Surface

RESEARCH ARTICLE

10.1002/2014JF003203

On funneling of tidal channels

S. Lanzoni[1] and A. D'Alpaos[2]

[1]Department ICEA, University of Padua, Padua, Italy, [2]Department of Geosciences, University of Padua, Padua, Italy

Key Points:
- A morphodynamic model for the 3-D equilibrium morphology of tidal channels
- A linear landward decrease in channel width can describe channel funneling
- Model provides a useful tool for quantitative long-term tidal morphodynamics

Correspondence to:
S. Lanzoni,
stefano.lanzoni@unipd.it

Citation:
Lanzoni, S., and A. D'Alpaos (2015), On funneling of tidal channels, *J. Geophys. Res. Earth Surf.*, *120*, 433–452, doi:10.1002/2014JF003203.

Received 13 MAY 2014
Accepted 3 FEB 2015
Accepted article online 7 FEB 2015
Published online 11 MAR 2015

Abstract Tidal channels dissect the tidal landscape and exert a crucial control on the morphodynamic evolution of these landscapes. Improving our understanding of channel equilibrium morphology is therefore an important issue for both theoretical and practical reasons. We analyze the case of a tidal channel dissecting a relatively short, unvegetated tidal flat characterized by microtidal conditions and a negligible external sediment supply. The three-dimensional equilibrium configuration of the channel is determined on the basis of a hydrodynamic model, describing the cross-sectional distribution of the longitudinal bed shear stresses, coupled with a morphodynamic model retaining the description of the main physical processes shaping the channel and the adjacent intertidal platform. Both channel bed and width are allowed to adapt to the flow field so that an equilibrium altimetric and planimetric configuration is eventually obtained, when erosion becomes negligibly small, and asymptotically constant elevations are reached everywhere within the domain. Model results reproduce several observed channel characteristics of geomorphic relevance, such as the relationship between channel cross-sectional area and the flowing tidal prism, the scaling of the width-to-depth ratio with channel width, and the longitudinal distributions of bed elevations and channel widths. In analogy with empirical evidence from estuaries, tidal channel funneling is usually assumed to be described by an exponential trend . Our theoretical analyses, modeling results, and observational evidence suggest that a linear relationship also provides a good approximation to describe longitudinal variations in channel width for short tidal channels. Longitudinal bed profiles characterized by a strong planform funneling tend to attain an upward concavity, whereas a low degree of convergence implies an almost linear profile. Finally, the model allows one to analyze the influence of environmental conditions (sediment characteristics, basin size, tidal amplitude, etc.) on the geomorphological features of tidal channels (equilibrium cross-sectional area and bottom profile, width-to-depth ratios, and planform shape). Wider and deeper channels develop as the width of the domain increases, as the tidal amplitude increases, or as the mean platform elevation decreases. Conversely, narrower and shallower channels result from an increase in the critical shear stress for erosion or a decrease in the flow conductance. We thus believe that this model provides a useful tool for quantitative analyses of long-term morphodynamics of tidal landscapes.

1. Introduction

Tidal channels exert a primary control on the exchanges of water, sediment, and nutrients within tidal landscapes thus driving their ecomorphodynamic evolution. These characteristic features of the tidal landscape cut through tidal flats and salt marshes, furnish preferential pathways for flooding and drying of intertidal areas, and provide ecosystem services and functions [e.g., *Allen*, 2000; *Friedrichs and Perry*, 2001; *Savenije*, 2005; *Fagherazzi and Overeem*, 2007; *de Swart and Zimmerman*, 2009; *Hughes*, 2012; *Coco et al.*, 2013].

Over the last decade, a number of theoretical and modeling studies have been carried out which analyzed the morphodynamic evolution of tidal channels and their equilibrium morphology. Some of these studies focused on the equilibrium longitudinal bed profile for a given longitudinal distribution of channel widths [*Schuttelaars and de Swart*, 2000; *Pritchard et al.*, 2002; *Hibma et al.*, 2003; *Seminara et al.*, 2010; *Toffolon and Lanzoni*, 2010] and on the transitory leading to this equilibrium configuration [*Lanzoni and Seminara*, 2002; *Todeschini et al.*, 2008; *van der Wegen et al.*, 2008]. Other studies analyzed the equilibrium shape and size attained by a generic channel cross section subjected to a given tidal forcing [e.g., *Fagherazzi and Furbish*, 2001; *D'Alpaos et al.*, 2006, 2010]. An attempt to provide a three-dimensional description of the equilibrium morphology of a tidal channel and of the adjacent platform was proposed by *Townend* [2010]. This behavior-oriented model consisted of a planform described by an exponentially converging width and cross-sectional area imposed a priori, a low-water channel cross section parabolic in shape, and an intertidal flat profile.

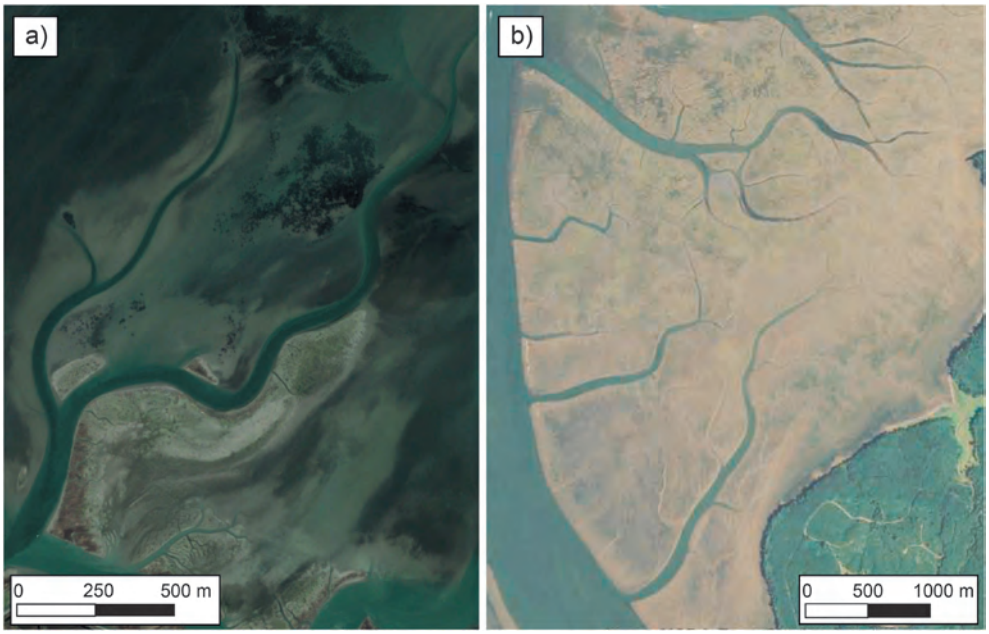

Figure 1. Examples of tidal channels dissecting the tidal flats of the (a) Venice Lagoon (Italy) and (b) Willapa Bay, WA (from Google Earth).

However, mathematical frameworks describing the three-dimensional equilibrium morphology of a tidal channel and of the adjacent intertidal platform without imposing a priori the form of characteristic channel properties, such as longitudinal variations of channel width and/or depth, are rare [*Canestrelli et al.*, 2007; *van der Wegen et al.*, 2008, 2010]. These studies investigated the long-term evolution of large estuarine systems, by using process-based numerical models solving the two-dimensional shallow water equations, the advection-diffusion equation for suspended load, and the bed evolution equation, with large computational effort. One limitation of these models, in fact, is that they would require a large number of time-consuming model runs to, for example, explore the influence of environmental conditions (e.g., sediment characteristics, geological constraints, and external forcing) on channel morphology, thus calling for modeling approaches of the type proposed here. Moreover, many of the above recalled studies focused on long estuarine systems or long tidal embayments [e.g., *Lanzoni and Seminara*, 2002; *Pritchard et al.*, 2002; *Canestrelli et al.*, 2007; *Todeschini et al.*, 2008; *van der Wegen et al.*, 2008] in which the free-surface oscillation is affected by inertia and friction, and, therefore, the effects related to the distortion of the tidal wave cannot be neglected. Here we focus on the equilibrium morphology of a single short tidal channel, for which a fast propagation and a negligible deformation of the tidal wave are ensured.

The aim of the present contribution, in fact, is to develop a process-based model in which the three-dimensional equilibrium configuration of the system formed by a channel and the adjacent tidal flat (Figure 1) is obtained as a result of the balance between erosion and deposition processes, driven by the flow field that becomes established in response to tidal forcing. The degree of the channel funneling, the longitudinal channel bed and tidal flat profiles, the shape and size of channel cross sections then result from the model rather than being externally imposed constraints. In addition, we analyze the influence of environmental conditions (e.g., sediment characteristics, geological constraints, and external forcing) on widely observed geomorphological features of tidal channels (longitudinal variations in channel width and depth, the size of channel cross sections and their relationship with the tidal prism, the width-to-depth ratio, etc.), an issue that previous studies failed to address as we shall note in the following.

Several authors have analyzed the power law relationship between channel cross-sectional area and the flowing tidal prism, for both inlet and sheltered sections, on the basis of theoretical analyses, observational evidence, process-based models, and laboratory experiments [e.g., *O'Brien*, 1969; *Jarrett*, 1976; *Marchi*, 1990; *Friedrichs*, 1995; *Rinaldo et al.*, 1999b; *Lanzoni and Seminara*, 2002; *D'Alpaos et al.*, 2009, 2010; *Stefanon et al.*, 2010; *van der Wegen et al.*, 2010]. However, departures from this power law, termed the O'Brien-Jarrett-Marchi law [*D'Alpaos et al.*, 2009], have also been documented for smaller sheltered

sections [e.g., *Friedrichs*, 1995; *Rinaldo et al.*, 1999b; *Lanzoni and Seminara*, 2002; *van der Wegen and Roelvink*, 2008; *D'Alpaos et al.*, 2010]. These departures have been interpreted either as a result of the transition between flood and ebb dominance within the same channel [*Friedrichs*, 1995], or as an artifact of the poor morphologic resolution of the data for smaller sections [*Rinaldo et al.*, 1999b], or as the effect of wetting and drying processes over the marsh surface [*Lanzoni and Seminara*, 2002; *D'Alpaos et al.*, 2010] leading to velocity peaks within the channels when the marsh platform is inundated or drained, or as the consequence of vanishing spatial tide residual sediment transport gradients [*van der Wegen et al.*, 2010]. Here we further explore the applicability to sheltered channel sections of this power law relationship, a valuable tool for long-term predictions of tidal morphodynamics [e.g., *D'Alpaos et al.*, 2007a].

One of the simplest measures of channel morphology is the width-to-depth ratio, β [*Allen*, 2000; *Marani et al.*, 2002; *Solari et al.*, 2002]. Although this ratio is a key factor for characterizing the three-dimensional morphology of a tidal channel [e.g., *D'Alpaos et al.*, 2005], a process-based relationship for predicting β as a function of environmental conditions (such as tidal forcing, sediment features, and geometry of the watershed served by a tidal channel) is still missing. Field observations carried out within the Venice Lagoon [*Marani et al.*, 2002] indicate that the width-to-depth ratio of salt marsh channels is usually much smaller than that of tidal flat channels, owing to the presence of vegetation and of relatively large fractions of cohesive sediments. Whether or not vegetation and sediment cohesion are the leading factors responsible for the different behavior of the width-to-depth ratio remains poorly understood, thus justifying further analyses.

Another striking feature of tidal channels is the remarkable variability experienced by their cross-sectional width, usually characterized by a rapid landward decrease [e.g., *Marani et al.*, 2002; *Davies and Woodroffe*, 2010; *Toffolon and Lanzoni*, 2010]. In particular, *Toffolon and Lanzoni* [2010] suggested that channel funneling is related to both the amount of tidal flats flanking the channel and the landward shoaling of the channel bed. The existence of a relationship between the equilibrium bed profile and channel width may be, however, related to the size and shape of both tidal channel cross sections and watershed area, an issue not yet clarified.

All the above mentioned channel morphological features are here analyzed by means of a suitably simplified model which retains the description of the main physical processes governing the morphology of tidal channels.

The model takes advantage of the observed relatively short length of tidal channels within coastal lagoonal environments [e.g., *Seminara et al.*, 2010; *Toffolon and Lanzoni*, 2010], allowing one to treat the tidal propagation quasi-statically and neglect the effects related to the distortion of the tidal wave. The cross-sectional distribution of the bed shear stresses, associated with the flowing discharge, is obtained by solving the longitudinal momentum equation for each section [*Fagherazzi and Furbish*, 2001; *D'Alpaos et al.*, 2006]. The erosion rates, calculated on the basis of the bed shear stress distributions, drive the temporal evolution of the bottom until an equilibrium configuration is attained, whereby each point within the domain attains an asymptotically constant elevation.

The paper is organized as follows. In section 2 we describe the morphodynamic model, focusing on the assumptions adopted to describe the hydrodynamic field and sediment transport processes, as well as the numerical approach used to solve the governing equations. Section 3 presents the results obtained by applying the model under different scenarios and compares relevant geomorphological features of modeled and observed tidal channels. Section (4) then follows, in which we address the key factors controlling longitudinal variations in channel width. Finally, section 5 draws a set of conclusions and suggestions for future research.

2. The Morphodynamic Model

2.1. Hydrodynamic Model

We set up a general modeling framework for the analysis of the morphodynamic evolution of a straight tidal channel, flanked by an intertidal platform. For the sake of simplicity, we assume that the tidal channel dissects a rectangular basin of width B_T and upstream length L and further assume a sinusoidal forcing tide of amplitude a_0 and period T at the seaward boundary (Figure 2), where the longitudinal coordinate, x, directed landward, originates. The channel is assumed to be short enough, such that at every instant, t, of the tidal cycle the discharge flowing through a given transect, $Q(x, t)$, can be calculated on the basis of a

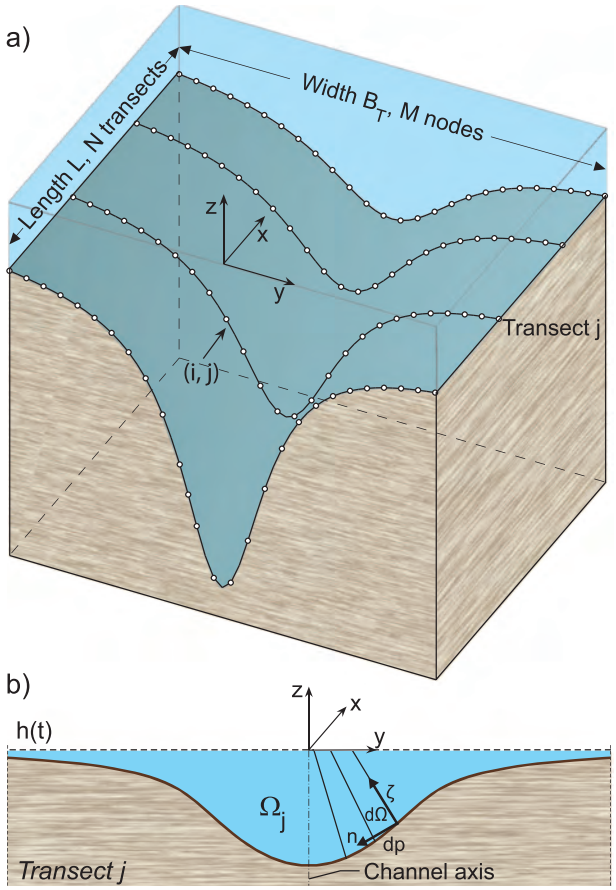

Figure 2. Sketch of the modeled tidal domain and notations. (a) Three-dimensional view of the computational domain at a given instant of the evolution; (b) cross-sectional representation of a generic transect.

quasi-static model [e.g., *Boon*, 1975; *Fagherazzi and Furbish*, 2001; *D'Alpaos et al.*, 2006]:

$$Q(x,t) = \frac{dV}{dt} \tag{1}$$

where $V(x,t)$ is the instantaneous volume of water upstream of the transect,

$$V(x,t) = \int_A [H(t) - \eta]\, dA \tag{2}$$

with $H(t) = a_0 \cos(\omega t)$ the instantaneous water level, assumed to be constant within the basin, $\omega = 2\pi/T$, $\eta(x,y,t)$ the local bed elevation, and A the area of the tidal watershed drained by the considered transect. The modeling framework provided by equations (1) and (2) holds for relatively short tidal channels such as those which usually dissect coastal lagoons [*Seminara et al.*, 2010; *Toffolon and Lanzoni*, 2010] and allows us to account for concentration of water flux and velocity peaks within the channel [e.g., *Boon*, 1975; *Friedrichs*, 1995; *Rinaldo et al.*, 1999b; *Fagherazzi and Furbish*, 2001; *D'Alpaos et al.*, 2006] due to wetting and drying processes which occur when the intertidal platform is inundated or emerges, respectively, during the tidal cycle.

However, different from *Boon* [1975], *Fagherazzi and Furbish* [2001], and *D'Alpaos et al.* [2006], in the present contribution we also account for water volume variations related to the upstream funneling of the channel cross section and for the longitudinal gradients of platform elevation due, e.g., to the landward increase in the elevation of the areas flanking the channel. In addition, the planoaltimetric configuration controlling along-channel variations in the flow discharge is the result of channel evolution starting from an initially flat unchanneled bottom configuration. The initial configuration is characterized by a small incision along the longitudinal axis of the domain to favor flow concentration and channel initiation.

Modeling the morphodynamic evolution of a tidal channel requires us to estimate the local longitudinal bed shear stress τ at any instant of the tidal cycle. The form of the channel cross section, in fact, depends on the transverse distribution of τ which, in turn, determines how the longitudinal component of the velocity is redistributed across the section, eventually contributing to generate the flowing discharge, Q. In order to determine the transverse instantaneous distribution of τ (see Figure 2b), we describe the shape of the channel cross section through the curvilinear coordinate system (x, n, ζ), where x is the longitudinal coordinate, n is the transverse curvilinear coordinate (with origin at the channel axis), and ζ is the axis normal to the bed. Moreover, z is the vertical axis, pointing upward and x, y is the horizontal reference plane coinciding with mean sea level (msl). Lateral distances measured along different transverse coordinate surfaces are, in general, not equal when moving from one normal coordinate surface to another, this being due to the curvature of the transverse axis. The transverse metric coefficient h_n, defined as

$$h_n = 1 - \frac{\zeta}{R}, \quad R = -\frac{1}{\cos\alpha}\frac{\partial^2 D}{\partial n^2}, \quad \cos\alpha = \sqrt{1 - \left(\frac{\partial D}{\partial n}\right)^2}, \tag{3}$$

accounts for this fact. Here R is the local radius of curvature of the transverse bed profile, α the angle that the vertical z forms with the normal to the bed coordinate ζ, and D is the instantaneous local flow depth. The longitudinal momentum equation, averaged over turbulence, then takes the form

$$\frac{\partial u}{\partial t}+u\frac{\partial u}{\partial x}+\frac{v}{h_n}\frac{\partial u}{\partial n}+w\frac{\partial u}{\partial \zeta}=-\frac{\partial}{\partial x}\left(\frac{p}{\rho}+gh\right)+\frac{1}{\rho h_n}\left[\frac{\partial(h_nT_{xx})}{\partial x}+\frac{\partial T_{nx}}{\partial n}+\frac{\partial(h_nT_{\zeta x})}{\partial \zeta}\right]-\frac{v^2+T_{nn}}{h_n}\frac{\partial h_n}{\partial x} \tag{4}$$

where u, v, and w are the components of the velocity along x, y, and z, respectively, p is pressure, ρ is water density, g is the gravitational constant, h is the elevation with respect to a given datum, and T_{xx}, T_{nx}, and $T_{\zeta x}$ the components of the stress tensor along x and T_{nn} is the n component of the stress tensor along n.

We observe that in the problem at hand (i) the horizontal scale of the relevant hydrodynamic processes largely exceeds the flow depth, and therefore, the gradient of the pressure head $(\partial(p/\rho g+h)/\partial x)$ can be replaced with the water surface gradient $(\partial H/\partial x)$; (ii) the flow field varies slowly in time, thus allowing us to neglect the local acceleration term, $\partial u/\partial t$; (iii) the flow field is essentially unidirectional, and secondary currents may thus be neglected in a first-order analysis; (iv) longitudinal gradients of the metric coefficient, h_n, are negligible; and (v) variations experienced by the bed shear stresses in the longitudinal direction are much smaller than those occurring in the transverse and vertical directions.

On the basis of the above assumptions, we integrate equation (4) along ζ, from the bed ($\zeta=\zeta_0$) to the free surface ($\zeta=D_\zeta$, where $D_\zeta=D/\cos\alpha$ is the distance of the water surface from the bed), and impose the kinematic and dynamic boundary conditions at the water surface and at the bed

$$\left[\frac{\partial D_\zeta}{\partial t}+u\frac{\partial D_\zeta}{\partial x}+\frac{v}{h_n}\frac{\partial D_\zeta}{\partial n}-w\right]_{\zeta=D_\zeta}=0,\qquad \left[\frac{\partial \zeta_0}{\partial t}+u\frac{\partial \zeta_0}{\partial x}+\frac{v}{h_n}\frac{\partial \zeta_0}{\partial n}-w\right]_{\zeta=\zeta_0}=0, \tag{5}$$

$$\left[T_{\zeta x}-\frac{1}{h_n}\frac{\partial D_\zeta}{\partial n}T_{nx}-T_{xx}\frac{\partial D_\zeta}{\partial x}\right]_{\zeta=D_\zeta}=0,\qquad \left[T_{\zeta x}-\frac{1}{h_n}\frac{\partial \zeta_0}{\partial n}T_{nx}-T_{xx}\frac{\partial \zeta_0}{\partial x}\right]_{\zeta=\zeta_0}=\tau \tag{6}$$

Further assuming that the magnitude of the velocity vector can be approximated by the cross-sectionally averaged flow velocity, U_Ω [*Lundgren and Jonsson*, 1964; *Parker*, 1978], allows us to obtain the following equation for the longitudinal bed shear stress $\tau(x,n,t)$

$$\tau=\rho gS\frac{d\Omega}{dn}+\frac{d}{dn}\int_{\zeta_0}^{D_\zeta}T_{nx}\,d\zeta \tag{7}$$

where $S=-\partial\left(H+U_\Omega^2/2g\right)/\partial x$ is the longitudinal energy slope, $d\Omega$ is the cross-sectional area between two normals to the bed (see Figure 2b), and

$$\frac{d\Omega}{dn}=\int_{\zeta_0}^{d_\zeta}h_n d\zeta. \tag{8}$$

Equation (7) was considered by *Glover and Florey* [1951] and *Pizzuto* [1990] in a fluvial setting and was subsequently adopted by *Fagherazzi and Furbish* [2001] and *D'Alpaos et al.* [2006] to model the cross-sectional evolution of a tidal channel. It assumes that the distribution of shear stresses across the section is determined by the balance between the resistive force, the downstream component of the weight of the water, and the lateral transport rate of downstream momentum due to turbulent stresses [*Parker*, 1978]. As stated above, equation (7) does not account for secondary currents, as those possibly generated by the exchange of water at the boundary between the channel and the adjacent tidal flat, progressive widening of the channel section, and curvature of the channel axis.

Finally, we observe that equation (7) allows us to compute, at any instant of the tidal cycle, the cross-sectional distribution of the longitudinal bed shear stress, $\tau(x,n,t)$, needed to evolve the bed, and of the corresponding depth-averaged velocity, $U(x,n,t)$, needed to compute an estimate, $Q^*(x,t)$, of the discharge flowing across a given transect, which depends on the unknown value of the energy slope. The estimate of the discharge, $Q^*(x,t)$, is then compared with the value $Q(x,t)$ provided by equation (1) to

determine iteratively the energy slope S. Starting from a guess value of S, we compute the quantity Q^*: if this value is higher (lower) than the actual value Q, we reduce (increase) the value of S until convergence is attained, i.e., $|Q^* - Q|$ is smaller than a given tolerance [see also *Fagherazzi and Furbish*, 2001].

In order to solve equation (7), we need to specify T_{nx}. Assuming that turbulent stresses prevail in determining the stress tensor, and adopting a classical Boussinesq eddy viscosity closure, the components of the stress tensor of normal x read

$$\left(T_{xx}, T_{nx}, T_{\zeta x}\right) = \rho\, \nu_T \left(\frac{\partial u}{\partial x}, \frac{1}{h_n}\frac{\partial u}{\partial n}, \frac{\partial u}{\partial \zeta}\right) \tag{9}$$

On the other hand, introducing the dimensionless coordinate $\hat{\zeta} = \zeta / D_\zeta$, which varies in the interval $[0, 1]$, we assume that the distributions along the normal to the bed of the eddy viscosity ν_T and of the longitudinal velocity u take the form

$$\nu_T(\hat{\zeta}) = u_* D_\zeta \mathcal{N}(\hat{\zeta}), \qquad u(\hat{\zeta}) = \frac{U}{C_{\text{ond}}} \mathcal{F}(\hat{\zeta}) \tag{10}$$

where $\mathcal{N}(\hat{\zeta})$ and $\mathcal{F}(\hat{\zeta})$ are suitable dimensionless functions, u_* $(= (\tau/\rho)^{0.5})$ is the friction velocity, U the depth-averaged velocity, and C_{ond} $(= U/u_*)$ is the local value of the flow conductance. This dimensionless quantity is given by the ratio $\chi/\sqrt{g}$, where $\chi = K_s R_h^{1/6}$ is the Chézy friction coefficient, K_s is the Strickler friction coefficient, and R_h is the local value of the hydraulic radius.

Recalling equation (9) and substituting equation (10) into (7), we finally obtain

$$\tau = \rho g S \frac{d\Omega}{dn} + \frac{1}{2}\frac{d}{dn}\left(\mathcal{I}\, C_{\text{ond}} D_\zeta^2 \frac{d\tau}{dn}\right) \tag{11}$$

with

$$\mathcal{I} = \int_0^1 \mathcal{N}(\hat{\zeta})\, \mathcal{F}(\hat{\zeta})\, d\hat{\zeta} \tag{12}$$

Note that the integral $\mathcal{I}$ depends implicitly on the transverse coordinate n, through the conductance C_{ond}, which affects the shape of the function $\mathcal{F}$. Indeed, assuming for ν_T a typical parabolic distribution, we obtain

$$\mathcal{N}(\hat{\zeta}) = \kappa\, \hat{\zeta}(1 - \hat{\zeta}) \tag{13}$$

and, consequently, the function $\mathcal{F}$ reads

$$\mathcal{F}(\hat{\zeta}) = \frac{1}{\kappa}\left(\ln \frac{\hat{\zeta}}{\hat{\zeta}_0}\right) \tag{14}$$

where $\hat{\zeta}_0 = \exp(-\kappa\, C_{\text{ond}} - 1)$ is the reference distance from the bed, ensuring that the depth-averaged velocity is equal to its mean value U, and κ is the von Karman constant. The integral $\mathcal{I}$ provided by equation (12) can be computed analytically as

$$\mathcal{I} = \frac{1}{6}\ln\left(\frac{1}{\hat{\zeta}_0}\right) - \frac{1}{9}\hat{\zeta}_0^3 + \frac{1}{4}\hat{\zeta}_0^2 - \frac{5}{36} \tag{15}$$

Substituting equation (15) into equation (11) and imposing that no momentum exchange occurs at the two lateral divides of the considered tidal basin, where the bed is approximately horizontal (i.e., $d\Omega/dn = D$ and $\tau = \rho g S D$), allows us to compute the cross-sectional distribution of the bed shear stress.

2.2. Sediment Balance

The temporal evolution of the local bed elevation $\eta(x, y, t)$ (referenced to msl) is governed by the classical two-dimensional sediment balance equation [e.g., *Seminara*, 1998]

$$(1 - \varphi)\frac{\partial \eta}{\partial t} + \frac{\partial (CD)}{\partial t} + \nabla \cdot \mathbf{Q}_s = 0 \tag{16}$$

where φ is the sediment bed porosity, C is the local instantaneous depth-averaged suspended sediment concentration, D is the local instantaneous flow depth, and $\mathbf{Q}_s$ is the total volumetric sediment flux, given

by the sum of bed load ($\mathbf{Q}_{sb}$) and suspended load ($\mathbf{Q}_{ss}$). We note that in estuarine environments sediment transport is typically dominated by suspended load. Further recalling that difference between local erosion and deposition fluxes, $Q_e - Q_d$, computed through the advection-diffusion equation for C, is given by the sum of the temporal variation of the sediment suspended in the water column, $\partial(CD)/\partial t$, and the divergence of the suspended sediment flux, $\nabla \cdot \mathbf{Q}_{ss}$, equation (16) can be eventually rewritten in the form [*Pritchard et al.*, 2002; *D'Alpaos et al.*, 2007a; *Toffolon and Lanzoni*, 2010]

$$\frac{\partial \eta}{\partial t} + \frac{1}{1-\varphi}(Q_e - Q_d) = 0 \tag{17}$$

The net flux $Q_e - Q_d$ is determined by a continual, dynamic adjustment between the fluid forces applied to the sediment bed and the condition of the bed itself [*Sanford*, 2008]. In principle, modeling of the evolution of fine and mixed sediment beds should account not only for sediment composition but also for (i) the vertical structure of the bed that, in turn, depends on its disturbance/recovery history and (ii) the effects of the biota that inhabit the bottom sediment. Although a few models have recently been developed that explicitly incorporate these factors into a dynamical framework for predicting fine-sediment bed evolution [*Sanford*, 2008], a widely used approach consists of assuming a mutually exclusive erosion and deposition behavior, with Q_d and Q_e estimated through the empirical relationships proposed by *Mehta* [1984] and *Einstein and Krone* [1962]:

$$Q_e = Q_{e0}\left(\frac{\tau}{\tau_e} - 1\right)\mathcal{H}(\tau - \tau_e) \tag{18}$$

$$Q_d = w_s C\left(1 - \frac{\tau}{\tau_d}\right)\mathcal{H}(\tau_d - \tau) \tag{19}$$

where Q_{e0} is a characteristic erosion rate, w_s is sediment settling velocity, τ_e and τ_d are the threshold shear stresses for erosion and deposition, respectively, and $\mathcal{H}$ is the Heaviside step function, which is 0 for negative arguments and 1 for positive arguments.

In general, the local value of the suspended sediment concentration, C, through the tidal cycle, should be determined by solving the 2-D advection-diffusion equation governing the suspended sediment balance [e.g., *Pritchard et al.*, 2002; *D'Alpaos et al.*, 2007a]. However, for flow fields that vary gradually with time (as in the case of tidal flows), a first-order approximation for C is provided by the classical solution [*Rouse*, 1937] resulting from the balance between vertical deposition and the mean upward flux associated with turbulent vertical diffusion. This occurs when the adaptation time (length) of the depth-averaged concentration can be assumed smaller than the time (length) scale of the considered problem. Such an assumption, together with the dilute character of the considered sediment suspension, suggests the possibility of neglecting the second term on the left-hand side of equation (16) and supports the use of the classical suspended load or total load predictors to evaluate $\nabla \cdot \mathbf{Q}_s$, when studying the equilibrium profile of tidal channels [*Lanzoni and Seminara*, 2002; *van der Wegen and Roelvink*, 2008].

Temporal and spatial variations in C, on the other hand, can produce deviations of the erosion and deposition fluxes from those computed by considering local hydrodynamics [*Bolla Pittaluga and Seminara*, 2003]. A delayed response of the concentration field to changes in flow velocity can be caused by the finite time which a sediment particle takes to settle out of suspension, during which the particle is carried for some distance after the local fluid velocity has fallen below the threshold for deposition (settling lag). This causes a hysteresis in the response of C to flow velocities [*Pritchard and Hogg*, 2003], which is accentuated if the threshold velocity for erosion is higher than that for deposition (scour lag). To account for these higher-order effects, the two-dimensional conservation equation for suspended sediment [e.g., *Pritchard et al.*, 2002; *D'Alpaos et al.*, 2007a] should be solved to evaluate the last two terms on the left-hand side of equation (16).

In the present work, we neglect possible vertical variations in erodibility due to sediment consolidation and the simultaneous erosion and deposition behavior suggested by some field observations [*Sanford and Halka*, 1993]. The quantities Q_{e0}, τ_e, and τ_d are thus assumed to depend only on the sediment grain size. We also do not consider the possible contributions of organic soil production and sediment capture by plant stems and leaves that arise when halophytic vegetation colonizes the bottom above a critical elevation

[e.g., *Morris et al.*, 2002; *Mudd et al.*, 2010], concentrating our attention on tidal channels carving unvegetated tidal flats. Finally, we restrict our analysis to the case of tidal environments, such as the lagoon of Venice, characterized by negligible external sediment supply so that no sediment can be imported to the system from rivers or from the sea and moderate rates of sea level rise [e.g., *Carbognin et al.*, 2004]. Before proceeding further, it is worth observing that this purely erosive scenario can also describe the evolution of tidal morphologies in the presence of a deposition rate that approximately balances the rate of sea level rise so that tidal channels develop for differential erosion. We recall that tidal landscapes characterized by small sediment supplies and rates of sea level rise are suggested to develop uniform intertidal platform elevations [*D'Alpaos*, 2011] and furthermore note that morphological changes associated with deposition processes act on a much smaller time scale than the time scale controlling channel incision. Indeed, field observations carried out by *D'Alpaos et al.* [2007b] in a salt marsh reconstructed within the lagoon of Venice emphasize that tidal channels can reach equilibrium in a few years, while several years (order of few decades) are needed to observe significant changes in intertidal platform elevations. Finally, we also note that the intensity of the erosion rate, quantified by Q_{e0}, does not affect the shape of the equilibrium state but determines the time required to reach it. Conversely, as we shall show in the following, the equilibrium morphology is strongly dependent on the characteristics of the sediment composing the bed, embodied by the value of the critical shear stress τ_e.

2.3. Numerical Approach

We consider a rectangular tidal basin described by N transects, each composed of M nodes. These nodes are spaced logarithmically along the transverse y direction in order to increase the density of nodes in the central portion of the domain where the channel is likely to develop (Figure 2). Each simulation starts by considering a nearly flat intertidal surface of average elevation η_{tf}, with a small incision (of amplitude 1 cm) along the longitudinal axis x [*D'Alpaos et al.*, 2006]. The value of η_{tf} can be taken as representative of the tidal flat equilibrium elevation that becomes established for given rate of sea level rise and external sediment supply.

The instantaneous discharge Q_j^k flowing at time t_k through the jth transect is computed as

$$Q_j^k = \frac{V_j^k - V_j^{k-1}}{t_k - t_{k-1}}, \tag{20}$$

with V_j^k the volume of water upstream of the jth transect at time t_k, given by

$$V_j^k = \sum_{m=2}^{j} \frac{\Omega_m^k + \Omega_{m-1}^k}{2} \Delta L_m, \tag{21}$$

where Ω_m^k and Ω_{m-1}^k are the cross-sectional areas at time t_k of two adjacent transects, m and $m-1$, located at a distance $\Delta L_m = x_m - x_{m-1}$. At the landward boundary ($m = 1$) we assume that the watershed area contributing to the channel head section is semicircular and, hence, characterized by an area $\pi B_T^2/8$.

The value of the bottom shear stress, τ_{ij}^k, at the ith node, the jth transect, and the instant t_k is computed by discretizing equation (11) through the procedure proposed by *Pizzuto* [1990] and determining iteratively the energy slope S_j (starting from a guess value of 0.0001) for which the total instantaneous discharge flowing through the jth transect equals Q_j^k (with a tolerance of 0.0001 m^3/s). The local flow conductance, $C_{\mathrm{ond}ij}^k$, is expressed through the Gauckler-Strickler friction law, $C_{\mathrm{ond}ij}^k = K_s R_{hij}^{k\,1/6}$. Since in the present contribution we restrict our attention to channels dissecting tidal flats, we do not consider vegetation effects and assume a constant value of the friction coefficient K_s, depending on the sediment grain size.

In order to avoid strong pulses of sediments at the beginning of each simulation, when significant differences occur between the initial nearly flat bed and the final equilibrium configuration, the amplitude of the forcing tide is increased progressively to the prescribed value a_0. The model is then run until an equilibrium planoaltimetric configuration of the entire basin is asymptotically attained (e.g., Figure 3). Equilibrium is assumed to be established when every point within the computational domain attains an asymptotically constant elevation in time. This condition implies that besides $Q_d = 0$, as assumed above, also Q_e tends to vanish everywhere in the computational domain. The issue concerning the conditions required by morphodynamic equilibrium is thoroughly discussed in section 4.

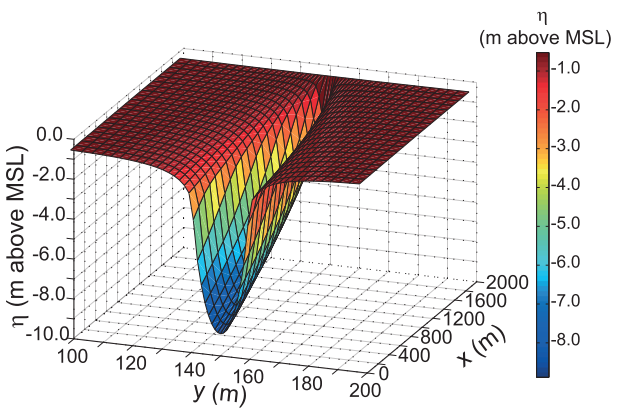

Figure 3. Three-dimensional view of equilibrium channel bathymetry attained at the end of run I3 (reference case; see Table 1). Values of the relevant parameters used in the simulation are as follows: $L = 2000$ m, $B_T = 300$ m, $a_0 = 0.5$ m; $\eta_{tf} = -0.5$ m above msl, $K_s = 30$ m$^{1/3}$ s^{-1}, $\tau_e = 0.4$ N m^{-2}, and $Q_{e0} = 0.0003$ kg m^{-2} s^{-1}.

At the end of each run, a mixed criterion combining thresholds on bed elevation and curvature [*Fagherazzi et al.*, 1999] is used to determine the position and characteristics (i.e., width, depth, and cross-sectional area) of the channel. Along a given transect, all the points with elevation below a threshold value (say 95% of the mean tidal flat elevation) and curvature smaller than a critical value (0.04 m^{-1}) are assumed to belong to the channel. The longitudinal distributions of channel width, $B(x)$, channel thalweg, η_{min}, and the mean channel bed elevation, $\eta_{avg}(x) = -D_{eq}(x)$, are finally determined. Note that D_{eq} coincides with the depth of the equivalent rectangular cross section of width B, computed with reference to msl.

3. Results

We performed several numerical experiments, listed in Table 1 with the corresponding parameters. We aimed at analyzing the influence of the following: (1) the width and length of the tidal basin, (2) the amplitude of the forcing tide, (3) the initial elevation of the intertidal platform drained by the channel, and (4) the properties related to bed sediment, such as the friction coefficient, K_s, and the critical shear stress for erosion, τ_e. Most of the tests were performed by varying, one at a time, model parameters starting from the reference case, I3, characterized by $L = 2000$ m, $B_T = 300$ m, $a_0 = 0.5$ m; $\eta_{tf} = -0.5$ m, i.e., 0.5 m below msl, $K_s = 30$ m$^{1/3}$/s, $\tau_e = 0.4$ N/m^2, and $Q_{e0} = 0.0003$ kg/m^2 s. A 100 year simulation with $N = 21$ transects and $M = 81$ nodes takes approximately 5 min using a modern desktop computer. For the range of parameters investigated, the model time interval needed to reach the final equilibrium channel elevation within a 5% error is of the order of 15–20 years. For all the equilibrium configurations emerging from the simulations, we analyzed the longitudinal profile of the mean channel bed elevation, the along-channel variation in channel width, the corresponding degree of channel funneling, and the longitudinal distribution of the width-to-depth ratio and of the tidal prism.

Before describing in detail the results of the simulations, it is worth discussing the general morphological tendencies resulting from the numerical experiments (Figure 4). When the width of the domain, B_T, increases from 100 to 500 m (keeping all the other parameters unchanged), both the tidal prism (the volume of water exchanged through a given cross section during half of tidal cycle, i.e., during flood or ebb) and the maximum discharge at a given cross section increase. This produces a deepening and a widening of the tidal channel (Figures 4a and 4b), while the maximum velocity remains unchanged and equal to the critical value for incipient sediment erosion. Similar trends (deeper and wider channels) are observed when the tidal amplitude, a_0, increases from 0.3 to 0.7 m (Figures 4c and 4d) or when the mean elevation of the tidal flats flanking the channel, η_{tf}, decreases from −0.1 to −1.0 m (Figures 4e and 4f). Importantly, if the tidal amplitude is too small (or platform elevation too high in the tidal frame), the length of the channel turns out to be shorter than the length of the basin. Increasing the critical shear stress for erosion, τ_e, from 0.2 to 0.6 N/m^2 (all the other parameters remaining unchanged) tends to produce narrower and shallower channels (Figures 4g and 4h). A similar trend is also observed decreasing the Strickler coefficient, K_s, from 20 to 40 m$^{1/3}$/s (Figures 4i and 4j). These morphological changes, however, do not affect appreciably the tidal prism, as well as the maximum discharge observed at each cross section. This is due to the fact that the maximum velocity within the channel tends to increase, thus compensating the observed decrease in channel cross-sectional area. Finally, we observe that increasing the length of the tidal basin (not shown in Figure 4) does not change the trend

Table 1. Values of the Relevant Parameters Adopted in the Simulations: L, Tidal Basin Length; B_T, Tidal Basin Width; η_{tf}, Initial Elevation of Intertidal Platform With Respect to MSL; a_0, Tidal Amplitude; τ_e, Critical Shear Stress For Erosion; and K_s, Gauckler-Strickler Friction Coefficient[a]

Run	L (m)	B_T (m)	η_{tf} (m)	a_0 (m)	τ_e (N/m^2)	K_s (m$^{1/3}$/s)
I1	2000	100	−0.5	0.5	0.4	30
I2	2000	200	−0.5	0.5	0.4	30
I3	2000	300	−0.5	0.5	0.4	30
I4	2000	400	−0.5	0.5	0.4	30
I5	2000	500	−0.5	0.5	0.4	30
II1	2000	300	−0.5	0.3	0.4	30
II2	2000	300	−0.5	0.4	0.4	30
II3	2000	300	−0.5	0.6	0.4	30
II4	2000	300	−0.5	0.7	0.4	30
III1	2000	300	−0.1	0.1	0.4	30
III2	2000	300	−0.3	0.3	0.4	30
III3	2000	300	−0.7	0.7	0.4	30
III4	2000	300	−1.0	−1.0	0.4	30
IV1	2000	300	−0.5	0.5	0.2	30
IV2	2000	300	−0.5	0.5	0.3	30
IV3	2000	300	−0.5	0.5	0.5	30
IV4	2000	300	−0.5	0.5	0.6	30
V1	2000	300	−0.5	0.5	0.4	20
V2	2000	300	−0.5	0.5	0.4	25
V3	2000	300	−0.5	0.5	0.4	35
V4	2000	300	−0.5	0.5	0.4	40
VI1	3000	450	−0.5	0.5	0.4	30
VI2	4000	600	−0.5	0.5	0.4	30
VI3	6000	900	−0.5	0.5	0.4	30
VI4	3000	75	−0.5	0.5	0.4	30
VI5	500	75	−0.1	0.5	0.4	30

[a]In all the simulations a tidal period of 12 h and a characteristic erosion rate $Q_{e0} = 0.0003$ kg/m^2 were considered. In addition, the tidal basin was described by considering $N = 21$ equally spaced transects, each one composed by $M = 81$ nodes.

characterizing the width distribution and the bed profile: simply, the channel continues to enlarge and becomes deeper as L increases. Indeed, at a given transect the tidal prism is not influenced by a downstream increase in the basin length.

In general, profiles characterized by a strong planform funneling (i.e., higher gradients of longitudinal channel width distribution) tend to attain an upward concavity (Figures 4a, 4b, 4e, and 4f), eventually tending toward a nearly constant depth [see *Toffolon and Lanzoni*, 2010, Figure 3]. Conversely, a low degree of convergence implies an almost linear profile. In order to rule out the effect of funneling, allowing the various bed profiles to collapse one over the other, the mean channel bed elevation, scaled by the amplitude of the forcing tide (i.e., η_{avg}/a_0), can be plotted as a function of the modified longitudinal coordinate ξ, introduced by *Toffolon and Lanzoni* [2010]. This dimensionless coordinate is defined as

$$\xi(\hat{s}) = \frac{1}{B(\hat{s})} \int_0^{\hat{s}} B_T(\psi)\, d\psi \qquad (22)$$

where ψ is an integration variable and $\hat{s} = s/L_l$ is the longitudinal coordinate, pointing seaward and originating at the channel head, s, scaled by the intrinsic length scale L_l. This latter quantity is defined as the ratio U_c/ω of the critical velocity for sediment erosion, U_c, to the tidal frequency, ω, and, hence, accounts (through U_c) for the physical properties of the sediment composing the bed. *Toffolon and Lanzoni* [2010] showed that for tidal channels that are much shorter than the tidal wavelength, such that inertial and frictional terms can be neglected in the momentum equation, the effects of width convergence and of the storage provided by lateral shoals can be implicitly accounted for through the modified longitudinal coordinate. As a consequence, the resulting profile does not depend on channel length but only on the amplitude and the period of the forcing tide, and the critical velocity for sediment erosion, therefore covering the whole range of possible equilibrium configurations. The form of the equilibrium profile, determined by considering a rectangular cross section of prescribed width $B(s)$ and imposing a balance between deposition and erosion, reads

$$D_{eq}(\xi) = a_0 \frac{1+\xi^2}{\sqrt{1+2\xi^2}} \qquad (23)$$

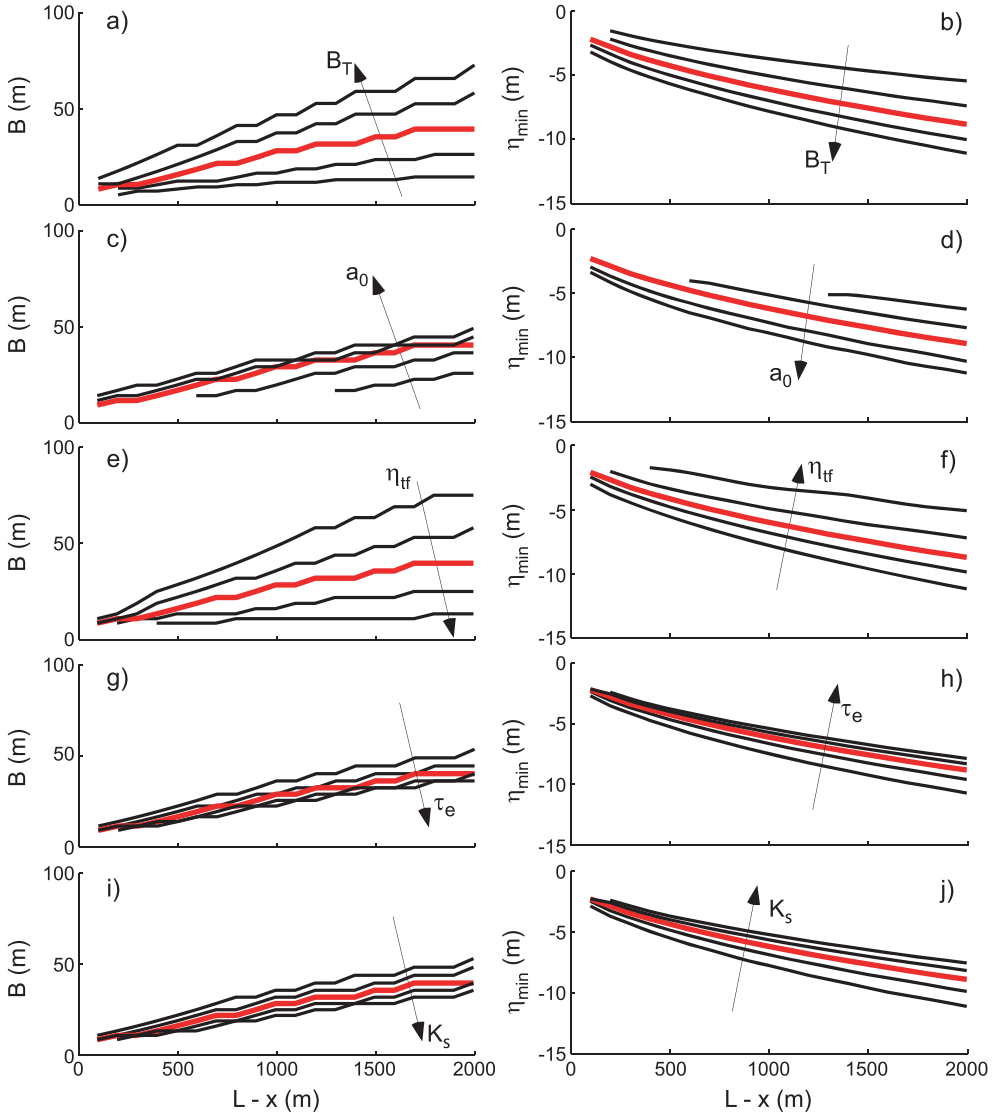

Figure 4. Longitudinal distributions of the cross-sectional width, B, and of the channel thalweg, η_{min}, characterizing the equilibrium morphology resulting from the numerical experiments. Effects of changes in a given parameter (all the others remaining unchanged): (a and b) tidal basin width B_T (test series I), (c and d) tidal amplitude a_0 (test series II), (e and f) initial tidal flat elevation η_{tf} (test series III), (g and h) threshold for sediment erosion τ_e (test series IV), and (i and j) Gauckler-Strickler friction coefficient K_s (test series V). Arrows denote the increase in the investigated parameter; thicker red lines indicate the reference test, I3. Note that the stair-step behavior of channel width as function of the longitudinal coordinate emerges because width can only change by finite steps, due to the finite transverse grid resolution.

where D_{eq} is the equivalent flow depth computed with respect to msl. Figure 5a indicates that when the dimensionless flow depth, D_{eq}/a_0, is plotted versus ξ, the computed profiles (showed as a set of disconnected points for the sake of simplicity) generally collapse toward the solid line representing equation (23). Note that the curve representing equation (23) has been computed by using for U_c the value (~ 0.18 m/s) corresponding to the critical shear stress for erosion (0.4 N/m^2) used in tests represented by black circles. Points corresponding to tests carried out with a different value of τ_e (white circles) indicate that sediment properties, embedded in the choice of U_c, are possibly causing deviations from the theoretical bed profile given by equation (23). It is also worth noting that the theoretical profile was determined by assuming a tidal amplitude such that the minimum water level was just above the elevation of the intertidal platform.

Equilibrium profiles emerging from our numerical experiments are quite similar to those displayed by tidal channels in the Venice Lagoon (Figure 5b). Note that the value of τ_e adopted in most of the tests (0.4 N/m^2)

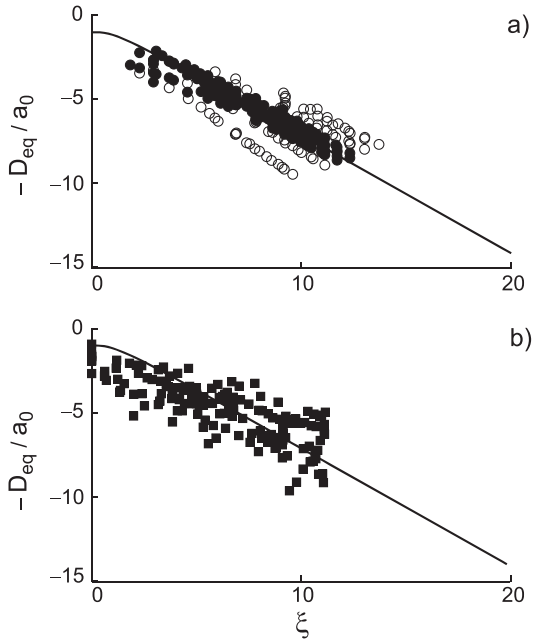

Figure 5. (a) The dimensionless equilibrium flow depths calculated with the present model as emerging from the numerical experiments are plotted versus the reduced coordinate ξ defined by equation (22). Black circles refer to test series I, II, and III, characterized by $\tau_e = 0.4$ N m^{-2}; white circles refer to test series IV, where τ_e varies in the range 0.2–0.6 N m^{-2}. (b) Dimensionless equilibrium flow depths emerging from bed profiles observed in a few channels in the northern part of the Venice Lagoon are plotted versus the coordinate ξ. The continuous line corresponds to the theoretical profile given by equation (23).

is equal to that typically determined from observations in the Venice Lagoon [see, e.g., *Amos et al.*, 2004] and is in line with what is expected for its sandy to silty bed sediments.

Further evidence supporting the reliability of the computed channel shapes and sizes is provided in Figure 6, which shows values of the tidal prism, P, versus channel cross-sectional area Ω obtained from the numerical simulations. The synthetically generated channel morphologies consistently show a tendency toward a power law relationship of the form $\Omega = k P^{6/7}$ along most of the channel, with a value of the proportionality constant $k = 2.6 \times 10^{-3}$ m$^{-4/7}$ quite close to values documented by *D'Alpaos et al.* [2010] for a number of channel cross sections within the Venice Lagoon (varying in the range $1–1.4 \times 10^{-3}$ m$^{-4/7}$). A slightly larger exponent of the power law is observed when wetting and drying processes characterize the intertidal platform flanking the channel (red diamonds in Figure 6a), which therefore is inundated or emerges, respectively, during the tidal cycle.

In addition, computed values of channel depth versus channel width shown in Figure 6b reproduce reasonably the trends observed in the Venice Lagoon by *Marani et al.* [2002], with smaller cross sections displaying an almost constant width-to-depth ratio, in the range 5–8, and larger sections characterized by depths varying in a narrow range of values and higher width-to-depth ratios. Note that a power law is also attained in the tests (red and magenta diamonds in Figure 6b) where the tidal amplitude is such that the intertidal platform flanking the channel dries during low tide, as typically occurs in salt marsh and shallow tidal flat channels. On the other hand, the plateau displayed by flow depths characterizing larger channels agrees with the tendency of a channel to develop an upward concavity (Figure 4), leading to a nearly constant depth channel as the degree of channel funneling increases [*Seminara et al.*, 2010; *Toffolon and Lanzoni*, 2010]. Our results compare favorably also with the results obtained by *Canestrelli et al.* [2007] who modeled the morphodynamic evolution of a single tidal channel by numerically solving the complete governing equations (blue triangles in Figure 6b).

As far as the form of the equilibrium cross section is concerned, a wide spectrum of geometries (U-shaped, V-shaped, rectangular-trapezoidal, and roughly right-angled triangular) is typically observed in nature, depending on the order of the channels within the tidal network and on the morphological tidal unit (i.e., salt marsh or tidal flat) served by the channel [*Allen*, 2000]. Smaller (low-order) salt marsh channels usually exhibit U-shaped or V-shaped narrow cross sections, with relatively low width-to-depth ratios ($\beta \sim 2–7$) [e.g., *Lawrence et al.*, 2004]. This geometry is suggested to be controlled by the interplay between cohesive sediment and vegetation dynamics [e.g., *Marani et al.*, 2002]. As the channel order within the tidal network increases, U-shaped forms are widely documented [*Allen*, 2000; *Lawrence et al.*, 2004]. These cross sections are less incised and, hence, characterized by larger width-to-depth ratios ($\beta \sim 8–50$ [*Marani et al.*, 2002]). The present model is indeed capable of qualitatively capturing the above described trends in width-to-depth ratios (Figure 6c), although the modeled cross sections are invariably characterized by gently sloping banks. The scaling of the width-to-depth ratio with channel width shown in Figure 6c clearly contains similar information compared to Figure 6b but emphasizes that β rapidly increases with B. Such a result bears important consequences, allowing one to determine β values when only channel width is known, e.g., from aerial and satellite images. Furthermore, we observe that also in this case the results obtained by

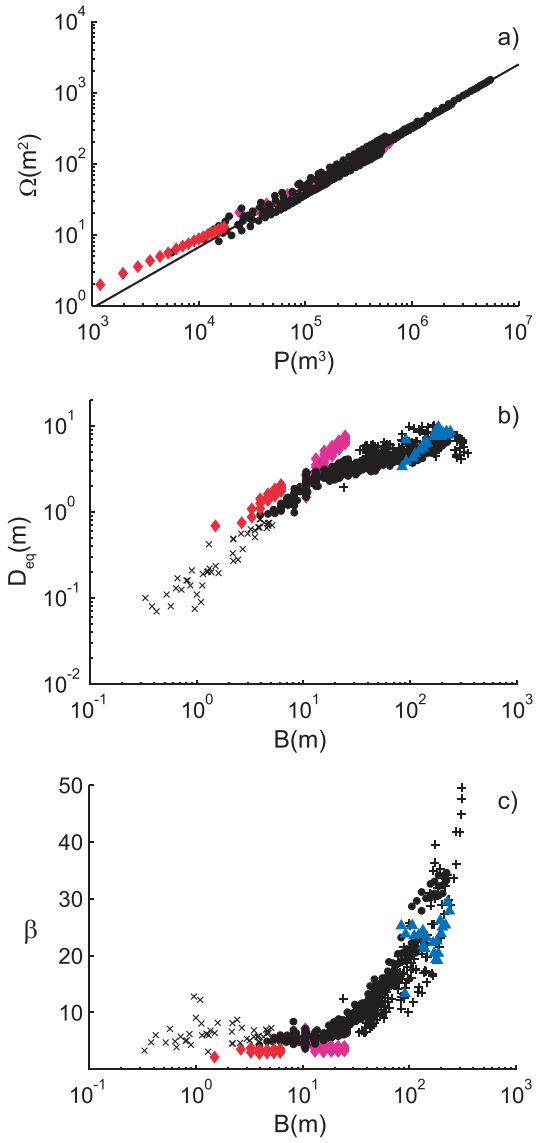

Figure 6. (a) Relationship between channel cross-sectional area and tidal prism. The continuous line represents the slope (6/7) of the O'Brien-Jarrett-Marchi law [*D'Alpaos et al.*, 2009]. (b) Channel depths and (c) width-to-depth ratios are plotted versus channel width for synthetic channel cross sections and for a number of actual sections surveyed in the Venice Lagoon. Crosses indicate two different salt marsh channels measured along their winding path; pluses indicate tidal flat channels [*Marani et al.*, 2002]. Black circles and diamonds denote the results of present simulations; diamonds refer to tests in which the elevation of the intertidal platform flanking the channel is just below (magenta diamonds) or well below (red diamonds) the minimum low tide level. Blue triangles refer to the numerical results of *Canestrelli et al.* [2007], obtained by solving the complete governing equations.

Canestrelli et al. [2007] support our findings. In addition, we note that because the model does not account for the role of vegetation or changes in sediment properties within the domain, the modeled characteristics of the smaller channels are a consequence of wetting and drying processes which affect the adjacent intertidal platform. Clearly, a quantitative comparison would require to account also for the effect of vegetation and sediment cohesion on channel bank stabilization. Nonetheless, model results are helpful in that they emphasize the role exerted by platform elevation within the tidal frame on the shape of channel cross sections, an issue which could not be highlighted on the basis of observational evidence.

4. Discussion

The degree of seaward cross-section enlargement experienced by tidal channels, in analogy with estuaries, is usually estimated by approximating the spatial width distribution by an exponential function of the form

$$B = B_0 \exp\left(\frac{s - L_C}{L_B}\right) \tag{24}$$

where B_0 is channel width at the mouth, L_C is channel length, and L_B is the convergence length. In the case of estuaries, this exponential trend is supported by empirical evidence [*Prandle and Rahaman*, 1980; *Lanzoni and Seminara*, 1998; *Savenije*, 2005] and by theoretical reasoning, for an ideal estuary in which friction and convergence effects tend to balance each other out. In fact, if spatial variations of both tidal range and maximum flow speed are small, the linearization of the governing equations (i.e., the 1-D de Saint Venant Shallow water equations) shows that the estuary behaves as an ideal one, where the depth keeps nearly constant and the width varies exponentially [*Pillsbury*, 1956; *Langbein*, 1963; *Savenije*, 2005].

In the case of tidal channels, however, the degree of channel funneling, measured by L_B, changes from channel to channel, depending on the complex interplay between the flow field within the channel and the erosion/deposition processes that control bank stability. The former is controlled by the geometry of storage areas, i.e., by the form and size of the watershed served by the channel, which is in turn determined by the overall structure of the tidal channel network.

The importance of the role of watershed morphology in controlling the aggregation of discharge within the channel and, hence, the degree of funneling, can be easily demonstrated as follows. If we consider the usual

one-dimensional mass conservation equation

$$B_T \frac{\partial H}{\partial t} + \frac{\partial (BUD)}{\partial s} = 0 \tag{25}$$

accounting (through B_T) also for the storage effects of intertidal areas flanking the channel, the discharge conveyed by the channel reads

$$Q(s) = BUD = -\int_0^s B_T \frac{\partial H}{\partial t}\, d\psi \tag{26}$$

The quasi-steady propagation of the tide that usually characterizes short channels in microtidal and mesotidal systems implies that water elevation, H, is a function of time, t, and is determined by the tidal forcing prescribed at the channel mouth [*Friedrichs and Aubrey*, 1994; *Schuttelaars and de Swart*, 1999; *Seminara et al.*, 2010], i.e., $H = a_0 \cos(\omega t)$ in the present case. The maximum discharge that has to be accommodated throughout the channel reads

$$Q_{\max}(s) = B(UD)_{\max} = a_0\, \omega \int_0^s B_T\, d\psi \tag{27}$$

The stage-discharge relationship typically observed in tidal channels [*Lawrence et al.*, 2004; *D'Alpaos et al.*, 2006; *Fagherazzi et al.*, 2008] indicates that $Q_{\max}$ is attained either at msl or when the intertidal areas (with elevation higher than msl) begin to dry, i.e., when the velocity tends to be maximum and a significant amount of water is still contained in the channel. Under equilibrium bed conditions, one can assume that the maximum velocity is approximately equal to the critical velocity for sediment erosion, while the flow depth takes the value D_{eq} computed with respect to msl. Channel width can then be estimated as

$$B(s) = \frac{a_0\, \omega}{U_c\, D_{\text{eq}}(s)} \int_0^s B_T\, d\psi \tag{28}$$

In the case considered here of a constant basin width B_T, provided that the equilibrium bed profile is described by equation (23), it turns out that the width should follow a linear distribution of the form

$$B(s) = \sqrt{\frac{2}{1+\sqrt{5}}}\, B_T\, \frac{s}{L_l} \tag{29}$$

and, hence, a linear profile may fit the along-channel width distribution.

Figure 7 shows the along-channel distributions of channel bed elevations and channel widths for the channels obtained through the present model, for a number of tidal channels in the Venice Lagoon and for the channels modeled by *Canestrelli et al.* [2007] and *van der Wegen et al.* [2008]. The present results show that although an exponential trend describes channel funneling with a reasonable approximation along most of the channel (middle column), a linear trend also nicely fits the data for both modeled and observed channel geometries (right column). It is worth noting that unless the degree of convergence is very strong, in the case of relatively short tidal channels, as those here considered, it is quite difficult to discriminate between a linear or an exponential relationship. Deviations from these trends usually occur toward the channel head and, hence, for the smaller order channels within a tidal network. This behavior agrees with the different degree of incision characterizing smaller channels, documented in Figure 6c. Interestingly, although *Canestrelli et al.* [2007] and *van der Wegen et al.* [2008] considered longer tidal channels in their numerical simulations, in both cases, a linear trend is found to reasonably fit the modeled channel geometries (right column).

Field observations also indicate that even though the degree of channel funneling changes from channel to channel with no apparent regularity, the values of the ratio L_B/L_C observed in different lagoons (Venice, Barnstable, and Petaluma) fall in a range (0.32–2.0 [*Marani et al.*, 2002]) comparable with that typically observed in tidal-dominated estuaries (0.19–1.99 [*Lanzoni and Seminara*, 1998]), with shorter channels being characterized by larger values. The ratio L_B/L_C resulting from modeled geometries attains values in the range 0.56–2.31 and conforms to the values (0.6–1.85) typical of tidal flat channels within the Venice Lagoon.

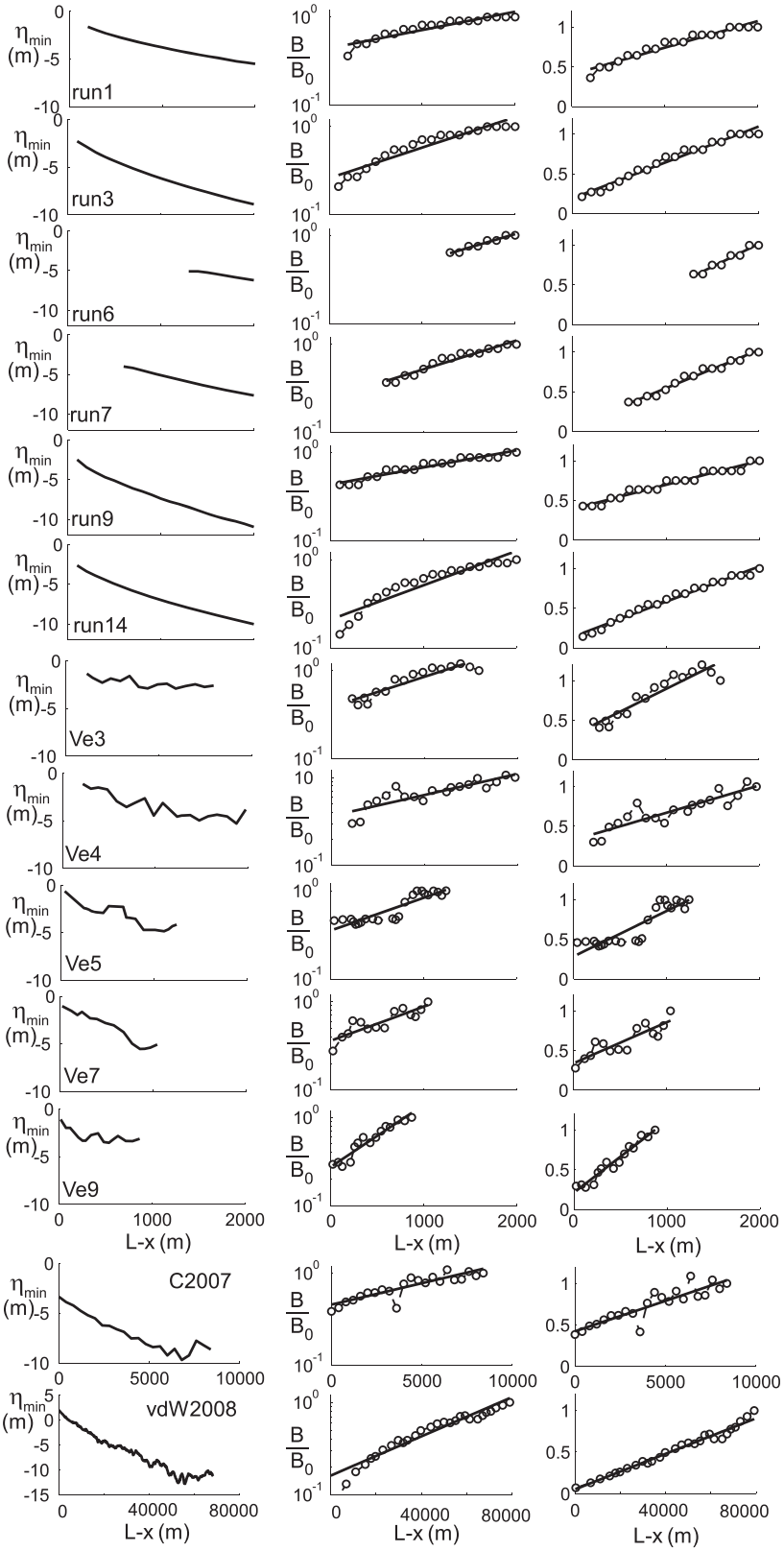

Figure 7. (left column) Along-channel distribution of channel bed elevation and of channel width, scaled by its inlet value, represented either (middle column) in a semilog plane or (right column) in a Cartesian plane. The plots denoted by run# refer to modeled configurations, those denoted by Ve# refer to actual tidal flat channels surveyed in the northern part of the Venice Lagoon, C2007 refers to *Canestrelli et al.* [2007], and vdW2008 refers to *van der Wegen et al.* [2008].

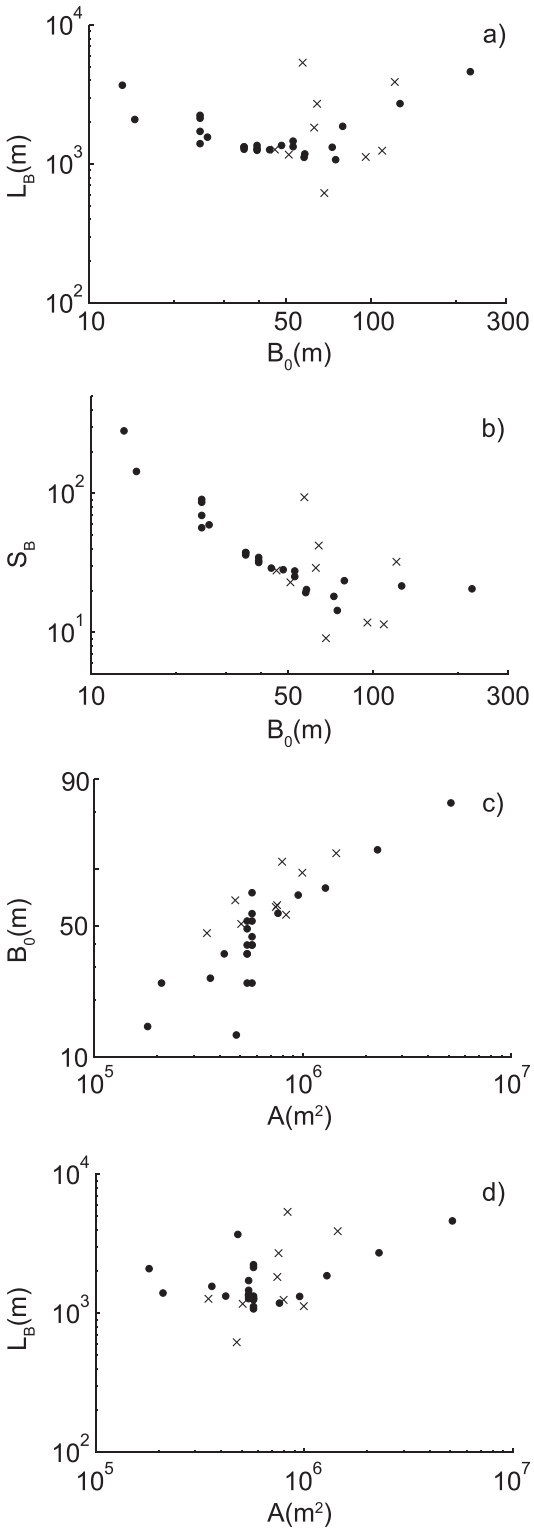

Figure 8. The inlet channel width B_0 is plotted versus (a) the convergence length L_B and (b) the funnel shape parameter S_B (= L_B/B_0). The watershed area A (= $B_T L_C$) is plotted versus (c) the inlet channel width B_0 and (d) the convergence length L_B. Black circles refer to model results; crosses refer to a set of nine tidal flat channels surveyed in the Venice Lagoon.

Other relevant features correctly reproduced by the model are those recently pointed out by *Davies and Woodroffe* [2010], on the basis of a detailed analysis carried out on a large number of tidal channels and estuaries in northern Australia. Their results indicate that the convergence length is weakly related to the local tidal range and to channel width at the mouth, B_0. Wider channels exhibit a visually stronger funnel shape than narrower channels and channels having a large catchment area relative to their mouth width are also characterized by larger L_B values. This latter observation is in accordance with *Rinaldo et al.*'s [1999a] suggestion that the seaward channel expansion is strictly linked to the development of drainage patterns leading to the formation of the dominant flow discharge. In particular, the presence of nonnegligible intertidal areas adjacent to the tidal channel (contributing to the increase in the tidal prism within the channel) should promote a wider channel.

All the above recalled morphological trends are reproduced by the present model. Figure 8a suggests the absence of a clear correlation between L_B and B_0. Conversely, Figure 8b supports the existence of a strong correlation between B_0 and the inverse of the funnel shape parameter S_B (= L_B/B_0), in accordance with the field data analysis described by *Davies and Woodroffe* [2010].

Finally, equation (28) indicates that a strong correlation should exist also between the inlet channel width and the watershed area A (= $B_T L_c$), as suggested by the geomorphic analysis of *Rinaldo et al.* [1999a]. Figure 8c shows that this geomorphological feature is nicely reproduced by the synthetically generated channel geometries. Less evident is the existence of a possible nonlinear relationship between L_B and A (Figure 8d). In general, it can be concluded that the funneling of short tidal channels is controlled by the geometry of the storage areas feeding the channel and by the longitudinal profile of the equilibrium bed. This result supports the speculation made by *Davies and Woodroffe* [2010] that in the absence of a significant nonchannel intertidal area, tidal processes alone seem unlikely to determine landward channel narrowing. Under equilibrium conditions, in fact, the maximum flood/ebb speed tends to remain nearly constant along the entire channel [*Lanzoni and Seminara*, 2002].

The results discussed so far refer to the case of purely erosional conditions and unvegetated intertidal areas. The model, however, can be

straightforwardly extended to include the effects of vegetation, through a proper modeling of the deposition rates due to the trapping effect of plant canopy and the belowground net organic production due to plant roots and rhizomes [see, e.g., *D'Alpaos et al.*, 2006].

One interesting question that might arise is whether a static or a dynamic morphological equilibrium can be attained. In the absence of any sediment exchange with the sea and/or sediment delivery from rivers, tidal channels achieve asymptotically a morphological equilibrium configuration provided that the residual sediment flux (averaged over a tidal cycle) eventually vanishes everywhere [*Lanzoni and Seminara*, 2002; *Tambroni et al.*, 2005; *Todeschini et al.*, 2008]. This condition is usually denoted as static equilibrium. Moreover, in the case of microtidal environments (in which the ratio of tidal amplitude to the characteristic channel depth is small) and short tidal channels (presupposing small distortions of the tidal wave) *Seminara et al.* [2010] demonstrated that equilibrium is attained with a more stringent static condition, whereby the sediment transport vanishes at each instant of the tidal cycle. In the case considered here, characterized by negligible external sediment supply ($Q_d = 0$), a static equilibrium condition is attained ($Q_e = 0$).

On the other hand, a condition in which both erosion and deposition occur, but balance each other (dynamic equilibrium), may exist when a certain amount of sediment (originating either within the lagoon or offshore) is imported/exported through the channel mouth [*Friedrichs and Aubrey*, 1996; *Pritchard and Hogg*, 2003]. In this case the longitudinal gradient of the residual sediment flux must vanish everywhere. For example, in the case of intertidal mudflats subject to the action of cross-shore macrotidal currents, *Pritchard et al.* [2002] have solved the advection-diffusion equation for C, showing that a static (i.e., fixed in time) equilibrium profile whereby no sediment is eroded or deposited at any point on the flat throughout the tidal cycle is attained when no sediment is externally supplied to the system. Conversely, in the presence of a constant far-field concentration imposed at the seaward boundary, the settling lag causes a net import of sediment which, in turn, leads to a shape of the tidal flat profile that is no longer changing while the flat, as a whole, advances seaward, accumulating sediment. In any case, the equilibrium flat profile tends to adjust such that the maximum current velocity is almost evenly distributed across it. We note that our model can be extended to consider the import of external sediment within the system, by prescribing the concentration at the channel mouth and solving at any instant of the tidal cycle the 2-D advection-diffusion equation for depth-averaged suspended sediment concentration C.

5. Conclusions

We developed a morphodynamic model describing the coupled altimetric and planimetric evolution of a tidal channel flanked by an intertidal platform, providing new insight on the processes determining the overall channel geometry at equilibrium. Different from previous studies, characteristic channel properties such as the degree of the channel funneling, the longitudinal bed profile, and the shape and size of channel cross sections, are not imposed a priori but are determined as a result of model simulations. Despite the simplifying assumptions used to derive it, the model proves reliable in reproducing, both qualitatively and quantitatively, several observed channel characteristics of geomorphic relevance. This bears important consequences for long-term simplified morphodynamic modeling approaches and for restoration issues, which rely on equilibrium formulations.

The O'Brien-Jarrett-Marchi law, relating channel cross-sectional area to the flowing tidal prism, is nicely followed by modeled morphologies. We emphasize that this geomorphic relationship holds for a wide range of channel sizes although smaller sections do not follow the power law. We argue that this is due to the effects of concentration of water flux and velocity peaks within the channel, which occur when the intertidal platform is inundated or emerges during the tidal cycle.

The relationship between width-to-depth ratio and channel width is also nicely reproduced by model results. The width-to-depth ratio is largely controlled by channel width. Smaller channels are characterized by more incised cross sections and by nearly constant width-to-depth ratios (in the range 5–8), whereas larger channels display larger width-to-depth ratios which rapidly increase with channel width. This different behavior is usually thought to depend on vegetation effects. The results of our modeling approach, in which the role of vegetation is not accounted for, allow us to show that an important role is also played by concentration of water flux and velocity peaks which usually characterize salt marsh and small tidal flat channels when the intertidal platform is inundated or emerges during the tidal cycle.

The computed longitudinal bed profiles are similar to those observed in the Venice Lagoon. These profiles tend to collapse on the theoretical relationship (equation (23)) derived by *Toffolon and Lanzoni* [2010], provided that sediment properties, embedded in the choice of the critical velocity for incipient erosion, are appropriately prescribed.

The model allows us to emphasize the influence of environmental conditions on typically observed geomorphological features of tidal channels. As the width of the domain increases, wider and deeper channels develop, whereas interestingly, the maximum velocity does not change and equals the critical value for incipient sediment erosion. Deeper and wider channels are also found to develop as the tidal amplitude increases or as the mean platform elevation decreases. An increase in the critical shear stress for erosion or a decrease in the flow conductance tend to produce narrower and shallower channels. The latter morphological changes, however, do not appreciably affect the tidal prism and the maximum discharge flowing through each cross section. This is due to the increase in the maximum velocity within the channel which compensates the observed decrease in channel cross-sectional area.

Tidal channel funneling is found to be reasonably described by an exponential relationship, as commonly observed in the literature. However, we do note that in many cases, a linear relationship also provides a good approximation to describe longitudinal variations of channel width, as suggested by theoretical analyses, modeling results, and observational evidence. In the case of our modeled geometries, this is likely related not only to the rectangular form of the watershed served by the tidal channel but also to the limited length of the channels which makes it difficult to discriminate between an exponential and a liner approximation. In any case, the overall comparison between computed and observed geometries is qualitatively and quantitatively satisfactory.

The degree of landward convergence is found to be strictly related to the geometry of storage areas feeding the channel and is therefore dictated by the development of drainage patterns leading to the formation of the dominant flow discharge. This influence is embodied by the strong correlations relating the channel inlet width to both the watershed area and the funneling parameter, defined by the ratio of convergence length to channel length.

We finally observe that the model is designed to directly incorporate other key mechanisms that could play a role in shaping channel geometry which have been neglected in this work. Watershed geometry, nonnegligible space-dependent rates of sediment deposition, the characteristics of silty sediments, vegetation encroachment on the intertidal platform, and the effect of overtides may nevertheless be described within the proposed framework in a relatively straightforward way.

Acknowledgments
This work was funded by the University of Padua project (CPDA103051) "Morphodynamics of marsh systems subject to natural forcing and climate changes." A.D. gratefully acknowledges the CARIPARO project titled "Reading signatures of the past to predict the future: 1000 years of stratigraphic record as a key for the future of the Venice Lagoon" and "Thetis Spa" for financial support. All the data for this paper are available and can directly be obtained from the figures.

References

Allen, J. R. L. (2000), Morphodynamics of Holocene salt marshes: A review sketch from the Atlantic and Southern North Sea coasts of Europe, *Quat. Sci. Rev.*, *19*(12), 1155–1231.

Amos, C. L., A. Bergamasco, G. Umgiesser, S. Cappucci, D. Cloutier, L. DeNat, M. Flindt, M. Bonardi, and S. Cristante (2004), The stability of tidal flats in Venice Lagoon—The results of in-situ measurements using two benthic, annular flumes, *J. Mar. Syst.*, *51*, 211–241.

Bolla Pittaluga, M., and G. Seminara (2003), Depth-integrated modelling of suspended sediment transport, *Water Resour. Res.*, *39*(5), 1137, doi:10.1029/2002WR001306.

Boon, J. D. (1975), Tidal discharge asymmetry in a salt marsh drainage system, *Limnol. Oceanogr.*, *20*, 71–80.

Canestrelli, A., A. Defina, S. Lanzoni, and L. DAlpaos (2007), Long-term evolution of tidal channels flanked by tidal flats, in *Proceedings of the 5th IAHR Symposium on River, Coastal and Estuarine Morphodynamics, Enschede, Netherlands, 17–21 Sept.*, edited by C. Dohmen and S. Hulscher, pp. 145–153, Taylor and Francis, London.

Carbognin, L., P. Teatini, and L. Tosi (2004), Eustacy and land subsidence in the Venice Lagoon at the beginning of the new millennium, *J. Mar. Syst.*, *51*, 345–353.

Coco, G., Z. Zhou, B. vanMaanen, M. Olabarrieta, R. Tinoco, and I. Townend (2013), Morphodynamics of tidal networks: Advances and challenges, *Mar. Geol.*, *346*, 1–16, doi:10.1016/j.margeo.2013.08.005.

D'Alpaos, A. (2011), The mutual influence of biotic and abiotic components on the long-term ecomorphodynamic evolution of salt-marsh ecosystems, *Geomorphology*, *126*, 269–278, doi:10.1016/j.geomorph.2010.04.027.

D'Alpaos, A., S. Lanzoni, M. Marani, S. Fagherazzi, and A. Rinaldo (2005), Tidal network ontogeny: Channel initiation and early development, *J. Geophys. Res.*, *110*, F02001, doi:10.1029/2004JF000182.

D'Alpaos, A., S. Lanzoni, S. M. Mudd, and S. Fagherazzi (2006), Modelling the influence of hydroperiod and vegetation on the cross-sectional formation of tidal channels, *Estuarine Coastal Shelf Sci.*, *69*, 311–324, doi:10.1016/j.ecss.2006.05.002.

D'Alpaos, A., S. Lanzoni, M. Marani, and A. Rinaldo (2007a), Landscape evolution in tidal embayments: Modeling the interplay of erosion sedimentation and vegetation dynamics, *J. Geophys. Res.*, *112*, F01008, doi:10.1029/2006JF000537.

D'Alpaos, A., S. Lanzoni, M. Marani, A. Bonometto, G. Cecconi, and A. Rinaldo (2007b), Spontaneous tidal network formation within a constructed salt marsh: Observations and morphodynamic modelling, *Geomorphology*, *91*, 186–197, doi:10.1016/j.geomorph.2007.04.013.

D'Alpaos, A., S. Lanzoni, M. Marani, and A. Rinaldo (2009), On the O'Brien-Jarrett-Marchi law, *Rend. Fis. Accad. Lincei.*, *20*, 225–236, doi:10.1007/s12210-009-0052-x.

D'Alpaos, A., S. Lanzoni, M. Marani, and A. Rinaldo (2010), On the tidal prism-channel area relations, *J. Geophys. Res.*, *115*, F01003, doi:10.1029/2008JF001243.
Davies, G., and C. D. Woodroffe (2010), Tidal estuary width convergence: Theory and form in North Australian estuaries, *Earth Surf. Processes Landforms*, *35*(7), 737–749.
de Swart, H. E., and J. T. F. Zimmerman (2009), Morphodynamics of tidal inlet systems, *Annu. Rev. Fluid Mech.*, *41*, 203–229, doi:10.1146/annurev.fluid.010908.165159.
Einstein, H. A., and R. B. Krone (1962), Experiments to determine modes of cohesive sediment transport in salt water, *J. Geophys. Res.*, *67*(4), 1451–1461.
Fagherazzi, S., and D. J. Furbish (2001), On the shape and widening of salt-marsh creeks, *J. Geophys. Res.*, *106*(C1), 991–1003.
Fagherazzi, S., and I. Overeem (2007), Models of deltaic and inner continental shelf landform evolution, *Annu. Rev. Earth Planet. Sci.*, *35*, 685–715, doi:10.1146/annurev.earth.35.031306.140128.
Fagherazzi, S., A. Bortoluzzi, W. E. Dietrich, A. Adami, S. Lanzoni, M. Marani, and A. Rinaldo (1999), Tidal networks: 1. Automatic network extraction and preliminary scaling features from digital terrain maps, *Water Resour. Res.*, *35*(12), 3891–3904.
Fagherazzi, S., M. Hannion, and P. D'Odorico (2008), Geomorphic structure of tidal hydrodynamics in salt marsh creeks, *Water Resour. Res.*, *44*, W02419, doi:10.1029/2007WR006289.
Friedrichs, C. T. (1995), Stability shear stress and equilibrium cross-sectional geometry of sheltered tidal channels, *J. Coastal Res.*, *11*, 1062–1074.
Friedrichs, C. T., and D. G. Aubrey (1994), Tidal propagation in strongly convergent channels, *J. Geophys. Res.*, *99*, 3321–3336.
Friedrichs, C. T., and D. G. Aubrey (1996), Uniform bottom shear stress and equilibrium hyposometry of intertidal flats, in *Mixing in Estuaries and Coastal Seas, Coastal Estuarine Stud.*, vol. 50, edited by C. Pattiaratchi, pp. 405–429, AGU, Washigton, D. C.
Friedrichs, C. T., and J. E. Perry (2001), Tidal salt marsh morphodynamics, *J. Coastal Res.*, *11*, 1062–1074.
Glover, R. E., and Q. L. Florey (1951), Stable channels profiles, *Hydraul. Lab. Rep., 325, Tech. Rep.*, U.S. Bureau of Reclamation, Washington D. C.
Hibma, A., H. M. Schuttelaars, and Z. B. Wang (2003), Comparison of longitudinal equilibrium profiles in idealized and process-based models, *Ocean Dyn.*, *53*(3), 252–269.
Hughes, Z. J. (2012), Tidal channels on tidal flats and marshes, in *Principles of Tidal Sedimentology*, edited by R. A. Davis Jr. and R. W. Dalrymple, pp. 269–300, Springer, Netherlands.
Jarrett, J. T. (1976), Tidal prism-inlet area relationships, *Gen. Invest. Tidal Inlets, Tech. Rep. 3*, U.S. Army Coastal Engineering Research Center, Fort Belvoir, Va., Army Engineer Waterways Experiment Station, Vicksburg, Miss.
Langbein, W. B. (1963), The hydraulic geometry of a shallow estuary, *Bull. Int. Assoc. Sci. Hydrol.*, *8*, 84–94.
Lanzoni, S., and G. Seminara (1998), On tide propagation in convergent estuaries, *J. Geophys. Res.*, *103*(30), 793–812.
Lanzoni, S., and G. Seminara (2002), Long-term evolution and morphodynamic equilibrium of tidal channels, *J. Geophys. Res.*, *107*(C1), 3001, doi:10.1029/2000JC000468.
Lawrence, D. S. L., J. R. L. Allen, and G. M. Havelock (2004), Salt marsh morphodynamics: An investigation of tidal flows and marsh channel equilibrium, *J. Coastal Res.*, *20*, 301–316.
Lundgren, H., and I. Jonsson (1964), Shear and velocity distribution in shallow channels, *J. Hydraul. Eng. Div.*, *90*(1), 1–21.
Marani, M., S. Lanzoni, D. Zandolin, G. Seminara, and A. Rinaldo (2002), Tidal meanders, *Water Resour. Res.*, *38*(11), 1225, doi:10.1029/2001WR000404.
Marchi, E. (1990), Sulla stabilitá delle bocche lagunari a marea, *Rend. Fis. Mat. Accad. Lincei*, *9*, 137–150.
Mehta, A. J. (1984), Characterization of cohesive sediment properties and transport processes in estuaries, in *Estuarine Cohesive Sediment Dynamics, Lect. Notes Coastal Estuarine Stud.*, vol. 14, edited by A. J. Mehta, pp. 290–315, Springer, New York.
Morris, J. T., P. V. Sundareshwar, C. T. Nietch, B. Kjerfve, and D. R. Cahoon (2002), Responses of coastal wetlands to rising sea level, *Ecology*, *83*, 2869–2877.
Mudd, S. M., A. D'Alpaos, and J. T. Morris (2010), How does vegetation affect sedimentation on tidal marshes? Investigating particle capture and hydrodynamic controls on biologically mediated sedimentation, *J. Geophys. Res.*, *115*, F03029, doi:10.1029/2009JF001566.
O'Brien, M. P. (1969), Equilibrium flow areas of inlets in sandy coasts, *J. Waterw. Harbors Coastal Eng. Div. ASCE*, *95*, 43–52.
Parker, G. (1978), Self-formed straight rivers with equilibrium banks and mobile bed: Part 2. The gravel river, *J. Fluid Mech.*, *89*(1), 127–146.
Pillsbury, G. (1956), *Tidal Hydraulics*, Corps of Engineers, Vicksburg, Miss.
Pizzuto, J. S. (1990), Numerical simulation of gravel river widening, *Water Resour. Res.*, *26*(9), 1971–1980.
Prandle, D., and M. Rahaman (1980), Tidal response in estuaries, *J. Phys. Oceanogr.*, *10*, 1552–1573.
Pritchard, D., and A. J. Hogg (2003), Cross-shore sediment transport and the equilibrium morphology of mudflats under tidal currents, *J. Geophys. Res.*, *108*(C10), 3313, doi:10.1029/2002JC001570.
Pritchard, D., A. J. Hogg, and W. Roberts (2002), Morphological modelling of intertidal mudflats: The role of cross-shore tidal currents, *Cont. Shelf Res.*, *22*, 1887–1895.
Rinaldo, A., S. Fagherazzi, S. Lanzoni, M. Marani, and W. E. Dietrich (1999a), Tidal networks: 2. Watershed delineation and comparative network morphology, *Water Resour. Res.*, *35*(12), 3905–3917.
Rinaldo, A., S. Fagherazzi, S. Lanzoni, M. Marani, and W. E. Dietrich (1999b), Tidal networks: 3. Landscape-forming discharges and studies in empirical geomorphic relationships, *Water Resour. Res.*, *35*(12), 3919–3929.
Rouse, H. (1937), Modern conceptions of the mechanics or turbulence, *Trans. Am. Soc. Civ. Eng.*, *102*, 463–543.
Sanford, L. (2008), Modeling a dynamically varying mixed sediment bed with erosion, deposition, bioturbation, consolidation, and armoring, *Comput. Geosci.*, *34*, 1263–1283, doi:10.1016/j.cageo.2008.02.011.
Sanford, L., and J. P. Halka (1993), Assessing the paradigm of mutually exclusive erosion and deposition of mud, with examples from upper chesapeake bay, *Mar. Geol.*, *114*, 37–57.
Savenije, H. H. G. (2005), *Salinity and Tides in Alluvial Estuaries*, 194 pp., Elsevier, Amsterdam.
Schuttelaars, H. M., and H. E. de Swart (1999), Initial formation of channels and shoals in a short tidal embayment, *J. Fluid Mech.*, *386*, 15–42, doi:10.1017/S0022112099004395.
Schuttelaars, H. M., and H. E. de Swart (2000), Multiple morphodynamic equilibria in tidal embayments, *J. Geophys. Res.*, *105*(C10), 24,105–24,118.
Seminara, G. (1998), Stability and morphodynamics, *J. Fluid Mech.*, *33*, 59–99.
Seminara, G., N. Tambroni, S. Lanzoni, and M. Toffolon (2010), How long are tidal channels?, *J. Fluid Mech.*, *643*, 479–494, doi:10.1017/S0022112009992308.
Solari, L., G. Seminara, S. Lanzoni, M. Marani, and A. Rinaldo (2002), Sand bars in tidal channels: Part 2. Tidal meanders, *J. Fluid Mech.*, *451*, 203–238, doi:10.1017/s0022112001006565.

Stefanon, L., L. Carniello, A. D'Alpaos, and S. Lanzoni (2010), Experimental analysis of tidal network growth and development, *Cont. Shelf Res.*, *30*, 950–962, doi:10.1016/j.csr.2009.08.018.

Tambroni, N., M. Bolla Pittalunga, and G. Seminara (2005), Laboratory observations of the morphodynamic evolution of tidal channels and tidal inlets, *J. Geophys. Res.*, *110*, F04009, doi:10.1029/2004JF000243.

Todeschini, I., M. Toffolon, and M. Tubino (2008), Long-term morphological evolution of funnel-shape tide-dominated estuaries, *J. Geophys. Res.*, *113*, C05005, doi:10.1029/2007JC004094.

Toffolon, M., and S. Lanzoni (2010), Morphological equilibrium of short channels dissecting the tidal flats of coastal lagoons, *J. Geophys. Res.*, *115*, F04036, doi:10.1029/2000JC000468.

Townend, I. (2010), An exploration of equilibrium in Venice Lagoon using an idealised form model, *Cont. Shelf Res.*, *30*, 984–999.

van der Wegen, M., and J. Roelvink (2008), Long-term morphodynamic evolution of a tidal embayment using a two-dimensional, process-based model, *J. Geophys. Res.*, *113*, C03016, doi:10.1029/2006JC003983.

van der Wegen, M., Z. Wang, H. Savenije, and J. Roelvink (2008), Long-term morphodynamic evolution and energy dissipation in a coastal plain, tidal embayment, *J. Geophys. Res.*, *113*, F03001, doi:10.1029/2007JF000898.

van der Wegen, M., A. Dastgheib, and J. Roelvink (2010), Morphodynamic modeling of tidal channel evolution in comparison to empirical PA relationship, *Coastal Eng.*, *57*, 827–837, doi:10.1016/j.coastaleng.2010.04.003.